Predictive Diagnosis of High-Power Transformer Faults by Networking Vibration Measuring Nodes With Integrated Signal Processing

Sergio Saponara, *Senior Member, IEEE*, Luca Fanucci, *Senior Member, IEEE*, Fabio Bernardo, and Alessandro Falciani

***Abstract*— This paper addresses the problem of predictive diagnostic in high-power transformers. Particularly, this paper is focused on their use in uninterruptible power supply systems for safety critical applications, such as railway interlocking signaling installations. With respect to the state of the art, where typically only thermal and electrical faults are monitored, this work proposes a distributed network of measuring nodes where also vibration-based mechanical stress diagnosis is implemented. Mechanical degradation is tracked through vibration measures, using multichannel accelerometers, with sensitivity down to 0.5 mg and local signal processing in the transformed frequency domain, up to 1 kHz. A compact hardware-software implementation of the nodes is also presented. The performances of the diagnostic system are assessed through experimental measurements on real three-phase high-power transformers used in railway applications.**

***Index Terms*— Electronic instrumentation, high-power transformers, power system measurements, predictive diagnosis, uninterruptible power supply (UPS), vibration/acceleration measurements.**

I. Introduction

PREDICTIVE maintenance is the holy grail for high power supply systems in industrial and transport applications [1]–[9], such as Oil & Gas or railway systems to name just a few, to avoid denial of service when a fault occurs. Such systems are made of a complex interconnection of several cabinets containing ac/dc and dc/dc converters, back-up battery, and/or super-capacitor modules for uninterruptible power supply (UPS). These power supply systems are characterized by multiphase currents of hundreds of amperes and voltages of hundreds of volts.

Due to safety reasons and to the high economical cost of unpredicted service interruption, the power supply system should be continuously working. Predictive maintenance [3] requires online measurements of key parameters of the system under analysis. Maintenance operations should be limited to the ordinary maintenance and synchronized, according to a predicted time schedule, with the maintenance of the whole system.

Manuscript received November 29, 2015; revised March 5, 2016; accepted March 31, 2016. Date of publication April 22, 2016; date of current version July 12, 2016. This work was supported by CEG Elettronica in the Framework of the Integrated Protection Power Supply Project through the FESR Program (Tuscany Region and European Commission). The Associate Editor coordinating the review process was Dr. Edoardo Fiorucci.

S. Saponara, L. Fanucci, and F. Bernardo are with the Dipartimento di Ingegneria dell'Informazione, University of Pisa, Pisa 56122, Italy (e-mail: sergio.saponara@iet.unipi.it).

A. Falciani is with CEG Elettronica spa, Bibbiena (Arezzo) 52011, Italy.

Color versions of one or more of the figures in this paper are available online at http://ieeexplore.ieee.org.

Digital Object Identifier 10.1109/TIM.2016.2552658

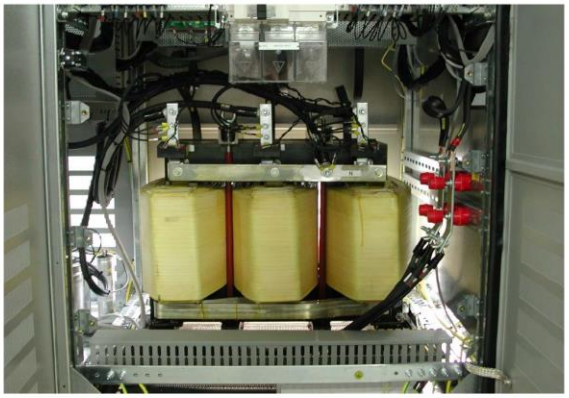

Fig. 1. Example of 120 kVA 50 Hz three-phase power transformer.

At the state of the art, the design for high reliability is based often on the use of redundant architectures and of components with high mean time before failure (MTBF). Such solutions lead to high system costs: high MTBF components are often expensive components and redundancy means increasing system size, weight, and cost.

A failure mode effects and criticality analysis [10], [11] study carried out on power supply systems for railway applications on real products provided by the CEG Elettronica industrial partner proved that key blocks for fault diagnosis are the power transformers used for power conversion and for isolation. They are typically three-phase transformers working at few tens of hertz (e.g., 50/60 Hz) with a weight up to 1000 kg, and several hundreds of kilovolt amperes [12]–[26]. In collaboration with CEG Elettronica, power transformers up to 350 kVA with a peak current higher than 1 kA and a weight higher than 850 kg have been designed and tested. For example, Fig. 1 shows a medium power 124 kVA dry-type transformer with a weight of 540 kg, 480 Vac at the primary side, and 250 Vac at the output (secondary), with peak current levels beyond 200 A. Several cabinets compose a real

power system, which contains multiple transformers. For other key blocks of power systems, such as capacitors and battery modules for UPS, online predictive diagnostic techniques have been already proposed in [27]–[31]. At the state of the art for UPS [32], [33], more mature valve regulated lead acid or NiCd cells are preferred to emerging lithium-based cells, for safety-critical railway power systems, due to their higher maturity, reduced cost and maintenance, and enhanced robustness in case of temperature higher than 60 °C [34].

In this work, we first propose a scalable power supply architecture with UPS capability for railway applications, highlighting the role and the possible positioning of power transformers. Then, we present a scalable network of measuring nodes, which for each cabinet acquire a multidimensional image of the transformer vibrations. Local signal processing in the frequency-transformed domain tracks the degradation of the vibration images that are correlated with the structural degradation of the transformers. Temperature, current, and voltage conditions are also measured to check thermal or electrical faults. All monitoring and processing nodes (MPNs) are interconnected through a controller area network (CAN) to a central unit supervising the whole system. USB and RF wireless connections are also available to increase system flexibility and scalability. Thousands of experimental measurements have been carried out on real power transformers to assess the validity of the new proposed diagnostic instrumentation.

Hereafter, Section II introduces a new power supply system with UPS capability for railway applications, highlighting the role and the positioning of power transformers. Section III shows the theoretical basis of vibration measurement to check power transformer degradation and highlights the specification for the predictive diagnostic system. Section IV proposes a hardware–software realization of the new instrument. Section V presents experimental measurements carried out on real power transformers and UPS for railway applications. Section VI presents a comparison of the proposed work with the state of the art. Conclusions are drawn in Section VII.

II. Architecture and Performance of Intelligent Power Supply System for Railway Applications

To ensure the safe movements of trains, in railway signaling applications, an interlocking system monitors the status of the objects in a railway yard, allowing or denying the movement of trains, in accordance with proper safety rules [35]. The availability and reliability of the interlocking system depend largely on the supply of electrical power, and hence, UPS capability is mandatory for railway power systems. UPS technology has evolved quickly over the past 20 years [32], [33]. The UPS designed in this work for railway applications provides a scalable solution with basic UPS modules from 10 up to 120 kVA and is therefore designed for both small and large railway installations. The system is packaged in cooled cabinets, such as in Fig. 2.

The proposed UPS scalable architecture is the combination of the power supply core in Fig. 3 plus power transformers whose possible positioning is shown in Fig. 4. A theoretical analysis of the optimal positions of power transformers in

Fig. 2. Cabinet for uninterruptable power supply system for railway.

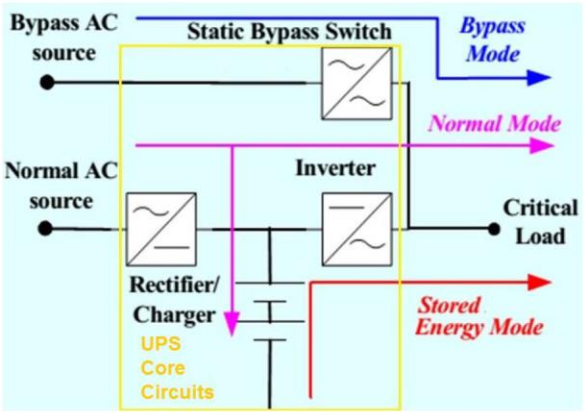

Fig. 3. Core of the UPS, double conversion topology working in normal, bypass, or stored energy modes.

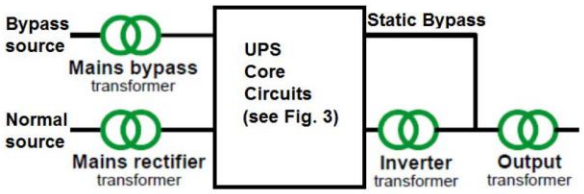

Fig. 4. Positioning of power transformers in a complete UPS system.

a UPS system, outside the scope of this paper, can be found in [36]. Each power transformer in Fig. 4 is represented by two overlapped circles (primary and secondary). The transformers in Fig. 4 are specifically dedicated to the UPS system. Therefore, in case the normal ac source in Fig. 3 is fed from an ac high voltage national power line, an extra separation transformer is present, not shown in Fig. 4. The main advantages obtained by using power transformers in UPS systems are the following:

1) the isolation they provide between output and source;
2) the voltage change that can be obtained by proper sizing the transformer ratio (this is necessary in applications where the mains voltage is not the same as the voltage used by the supplied equipment);
3) the impedance they provide, which limits fault currents or acts as a noise filter;
4) the blocking effect they provide against the 3rd, 9th, 15th, and other multiples-of-three harmonic currents.

The architecture in Fig. 4 is scalable, so that 16 different combinations can be realized. The mains transformers and the output transformer in Fig. 4 can be located either locally or remotely from the UPS. The effective combination of power transformers, used for a given UPS installation, depends on the performance to be achieved, on the desired redundancy level, and also on the target budget in terms of cost, size, and weight. For example, the inverter transformer in Fig. 4 provides the function of breaking the neutral connection between the rectifier and bypass inputs, but either a rectifier or a bypass transformer also provides this function. Therefore, the inverter transformer function is redundant if either a rectifier or bypass transformer is installed. Its use can be avoided if the application has stringent constraints in terms of weight, cost, and size.

After analyzing the use of the power transformers in the UPS system, hereafter we complete the description of the architecture presented in Figs. 3 and 4. Table I summarizes the most important parameters for its building blocks. The reported values in Table I refer to experimentally measured data in typical working conditions. Moreover, the UPS features very good dynamic response to load variations: in less than 10 ms, the instantaneous voltage returns to its ideal value. The proposed UPS is powered directly by low voltage mains or alternatively through a dc/ac conversion device in case the power supply line is fed from a dc high voltage national power line. The proposed UPS can also be powered from the high voltage ac power line. In such a case, as discussed before, an extra separation transformer is present. The output of one of these ac sources is the normal ac source in the core of the UPS whose schematic is reported in Fig. 3.

A generating set (GS) can also supply the UPS, bypass ac source in Fig. 3 with a by-pass switch and an ac/ac regulation. The functional independence between the GS source and the static UPS makes it possible to separate the two installations geographically and place the UPS close to the load, while, for example, the GS can be located in containers outside the station building. In the core of the UPS in Fig. 3, an inverter is connected in series between the ac input and the load, with power for the load flowing continuously through the inverter.

Three operating modes are possible in the UPS topology presented in Fig. 3, namely, normal, stored energy, and bypass. In normal mode, the load is continuously supplied by a rectifier-inverter combination, which carries out the double conversion (ac/dc, then dc/ac). The UPS goes into stored energy mode when the ac input fails or goes out of the specified tolerance range. The inverter and the battery continue to support the load under this mode. The UPS runs in stored energy mode until the stored energy is exhausted or the ac input returns to the specified tolerance level.

This type of UPS is equipped with a static bypass switch, allowing instantaneous transfer of the load to the bypass ac input. This switch is used in the event of a UPS internal malfunction, load current transients (in-rush, or fault clearing), prolonged overloads, or at the end of battery back-up (autonomy time). However, the presence of a bypass implies that the input and output frequencies and phase must be identical, and the voltage coordinated. The UPS is synchronized with the source of ac bypass supply to allow a transfer to bypass without any interruption.

TABLE I

MEASURED PARAMETERS FOR THE UPS BUILDING BLOCKS AND TYPICAL CONDITIONS

UPS SYSTEM	
Size (kVA)	***10 to 120***
Input Voltage (Vac)	400±15%
Input Freq. (Hz)	50÷60 Hz ± 5Hz
Input current distortion, nominal load %	27% with standard 6 pulses bridge
	10% with 12 pulses bridge
	5% with 12 pulses bridge + THD filter
Vdc	384
Output Voltage (Vac)	3x400+N
Output freq. (Hz)	50÷60 Hz ± 5Hz
Efficiency (%)	88 (at 10 kVA) to 93 (at 120 kVA)
RECTIFIER (AC/DC)	
Size (kVA)	***10 to 120***
Input voltage (Vac)	400±15%
Input current @ full load (A)	Max 262.4 (at 120 kVA)
Efficiency (%)	93 (at 10 kVA) to 97 (at 120 kVA)
BATTERY	
Size (kVA)	***10 to 120***
Cells Max Pb battery	Pb:174@380Vac - Pb:182 @400Vac
Cells Max Pb/e battery	Pb-e:192 @380Vac - Pb-e:200 @400Vac
Cells Max Ni-Cd battery	Ni-Cd:270 @380Vac - Ni-Cd:285 @400Vac
Floating Voltage Vdc	432
Max battery capacity (Ah), 1 h autonomy	470
Max recharge current(A)	114
INVERTER (DC/AC)	
Size (kVA)	***10 to 120***
Input Voltage (Vdc Range)	320-490
Input current (A)	20.6 (at 10 kVA) to 246.9 (at 120 kVA)
Input Power (kW)	8.9 (at 10 kVA) to 106.7 (at 120 kVA)
Efficiency (%)	95 (at 10 kVA) to 96 (at 120 kVA)
Output Voltage (Vac)	3x400+N
Voltage Stability (static)	1% static according to IEC 60146-1-1 IEC 60146-2
Voltage Stability (dynamic)	6% dynamic with reset to1% in 40ms according to IEC 60146-1-1 IEC 60146-2
THD Linear load	1,5% linear load according to IEC62040-3
THD No linear load	<5% with no linear load according to IEC62040-3
BYPASS LINE	
Size (kVA)	***10 to 120***
Input Voltage (Vac)	400±10%
Overload	130% (Pn) continuous; 2000%(In) 10ms

The proposed UPS is made of the following sections (see Table I for the main railway UPS parameters).

1) *Rectifier With Input Transformer:* The purpose of the rectifier section is to convert the ac voltage of the line to dc voltage for charging the batteries and to feed the next inverter section. The rectifier is three-phase 12-pulse silicon controlled rectifier made. An isolation and voltage adaptation transformer (mains rectifier transformer in Fig. 4) and inductors placed at the exit of the bridge conversion (dc side) reduce the distortion produced by the network rectifier and the ripple to the battery, thus ensuring its maximum duration. The rectifier is designed to supply simultaneously both the inverter in conditions of maximum load and the battery at the maximum charging current.

2) *Batteries:* Batteries are typical organized as a complex array of lead acid or NiCd basic cells. Thanks to their autonomy of several minutes, static UPS units reduce the carbon footprint related to operating on a GS. During a brief power outage, the bank of lead-acid or NiCd batteries provides current, eliminating the need to start the GS. This means fewer GS start-ups per year and a reduction in fuel consumption. This mode also improves power usage effectiveness on the installation as a whole by avoiding the necessary permanent warm-up as well as cooldown time (2–3 min) after each use of the GS during a micro-outage. To be noted that more mature lead acid or NiCd cells are preferred in Table I to emerging lithium-based cells, due to their higher maturity, reduced cost and maintenance, and enhanced robustness in the case of temperature higher than 60 °C [34]. Techniques for predictive diagnosis of the state-of-health of lead-acid and/or nickel-based cells are already available from [30] and [31]. Moreover, from the Failure Mode and Effect Analysis for railway signaling systems, it emerged as a key issue the prediction of power transformer degradation. This is why this work is focused on power transformer fault diagnosis, while for battery diagnosis the reader can refer the available literature [30], [31].
3) *Inverter:* The inverter converts the dc voltage Vdc supplied by the rectifier, or by the battery, into ac voltage, fully stabilized in frequency and amplitude. The inverter output voltage is generated with pulsewidth modulation (PWM) driving Insulated Gate Bipolar Transistor. The use of a high carrier frequency for the PWM and a dedicated filter circuit constituted by the ac transformer and capacitors ensures minimal distortion of the output voltage (Total Harmonic Distortion $< 2\%$ of linear loads). The output voltage of the inverter, controlled by the inverter control logic, ensures constant and equal voltage in the output of the UPS, even with unbalanced loads. The harmonic distortion in the output is kept low thanks to a unique technology adaptive correction, even with the application of loads highly distorted. For redundancy reasons, the inverter transformer in Fig. 4 is installed, unless a specific UPS application has stringent cost, size, and weight requirements. In such a case, the inverter transformer can be removed since its function is substituted by the use of the other transformers in Fig. 4.
4) *Bypass Line:* Normally, the inverter guarantees the power distribution. In the case of malfunctions or overload in the inverter, the bypass line supplies the load through the main static switch or directly (manual bypass). The three-phase voltage stabilizer maintains the nominal value of the output voltage within a 2% compared with a variation of the input voltage range between $\pm 10\%$ of the nominal value of the line. The insertion is fast and allows compensating for the rapid changes in voltage due, for example, to the inclusion of motors.
5) *Diagnostic:* The diagnostic system oversees the entire UPS system providing to manage testing and periodic checks, ensuring the operation of the equipment and promptly alerting in case of anomalies. This block exploits a predictive diagnostic strategy based on the monitoring unit presented in the next sections.

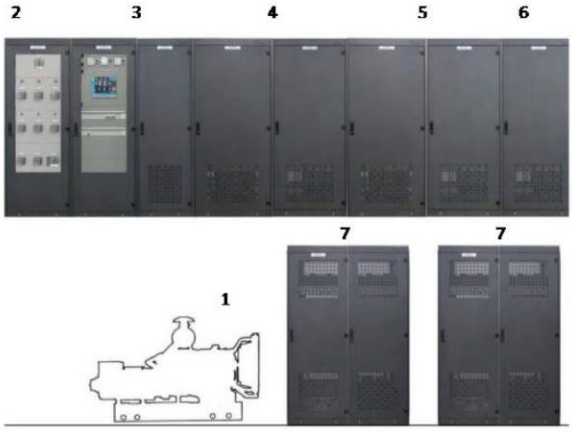

Fig. 5. Proposed power supply system for railway; networked cabinets of 1-GS; 2-switch between GS, the bypass ac source, and electrical energy provider, the normal ac source; 3 to 6-rectifiers and inverters; 7-batteries for UPS (lead acid/Ni-Cd used, lithium batteries foreseen in the future [34]).

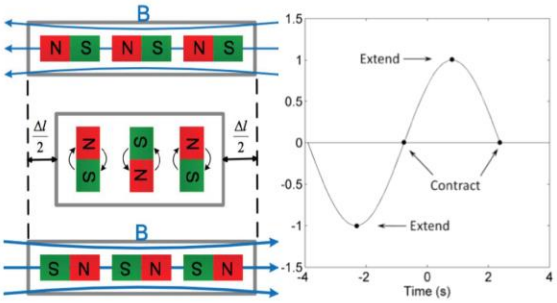

Fig. 6. Magnetostriction effect.

Fig. 5 presents a view of the cabinets of the complete UPS, obtained combining the schemes in Figs. 3 and 4, for railway signaling applications. Depending on the configuration of the specific UPS installation, power transformers of Fig. 4 may be included in cabinets 2–6.

III. Degradation in Power Transformers and Specifications for the Monitoring System

The main causes of degradations for high-power transformers can be of electrical nature (over-current and over-voltage conditions), of thermal nature (over-temperature), and of mechanical nature [magnetostriction forces (see Fig. 6) causing cyclic contract/extend events). State-of-the-art solutions often monitor current and/or voltage and/or temperature to avoid out-of-range dangerous values. Such techniques have been implemented also in our system but are not detailed in this paper. Indeed, this paper focuses on the innovative part of the system, which is the measurement and detection of mechanical degradation.

When ac currents, with peak values up to 1 kA, flow in the transformer windings, this causes magnetic forces, whose intensity is proportional to the square low of the current

$$F_{\text{mag}} \propto [I \cdot \sin(2\pi f_0 t)]^2. \quad (1)$$

Such forces are characterized by a fundamental frequency doubled (100/120 Hz) versus 50/60 Hz of the input ac current. These forces, continuously extending and contracting the mechanical structure of the transformer, cause a degradation of the transformer itself finally resulting in a fault of the system. At the state of the art, this mechanical degradation is checked through visual inspection or through acoustic analysis since vibrations are at hundreds of hertz. However, visible inspection or acoustic diagnosis allows to detect the fault too late, when the transformer is already damaged. Moreover, as proved by experimental measurements that we have carried out on real power systems, in the industrial environment where such systems are used the background acoustic noise level is at least in the range of 60/70 dB with frequencies from few hertz to kilohertz. Therefore, the acoustic effects of vibration degradation of the power components are detectable only after a big damage has occurred. For predictive diagnostic instead, a periodical monitoring is needed with a very high sensitivity allowing to detect the early signs of mechanical damage.

For the diagnosis of power transformers mechanical degradation, since the magnetostriction forces are proportional to the square of current, the main frequencies of interest are at double of the basic current frequency (e.g., 100/120 Hz for power systems at 50/60 Hz) and its multiple values. As proved by experimental results in Section V, to discriminate between a good-working power transformer and one with degradation, the frequencies beyond 1 kHz are not significant. Therefore, the frequency range of interest in this work is from 100 Hz to 1 kHz. The required sensitivity level for vibration measurements is as low as 0.5 mg. The dynamic range is up to several g (roughly four orders of magnitude from 0.5 mg to some g), being 1 g = 9.8 m/s^2. Each of the three phases of the transformer has to be monitored with vibrations that can be in each of the three (x, y, and z) spatial directions. Hence, at least a vector of nine measuring points for each transformer has to be acquired.

From a signal processing point of view, once an image of the vibrations of the power transformer is obtained, then an analysis in frequency domain is carried out. By continuously comparing the intensity level of the spectrum peaks up to 1 kHz with the same historical values stored in a nonvolatile memory, the transformer degradation versus time can be tracked. Fixing some heuristic thresholds, depending on the degradation level acceptable for the system user, a predictive diagnostic warning is send or not. Since a high power supply system for industrial and transport applications is composed by several of these blocks (see Fig. 5), all the measuring and processing nodes (MPNs) should be networked and connected to a central unit. The latter will supervise the alarms for the whole system. An industrial-grade networking technology has to be used.

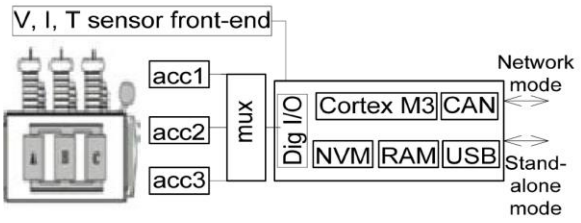

Fig. 7. Architecture of an MPN unit.

IV. Predictive Diagnostic System Implementation

The predictive diagnostic system is implemented as a CAN interconnection of monitoring and processing nodes, the MPN unit in Fig. 7. There is one MPN unit for each power transformer in the system, plus one central supervision unit. The latter has not specific constraints in terms of power consumption, size, and weight and hence can be realized stand-alone using an industrial PC.

For the MPN unit, a dedicated electronic design, at least at single printed circuit board (PCB) level, is needed to meet size and weight constraints and to avoid high overheads in terms of power consumption and cost.

The diagnostic system is interconnected through a CAN with a scalable complexity, from few nodes to tens of nodes and a maximum connecting distance scalable from 10 m to hundreds of meters. As target application, this work is focused on UPS installations for railway signaling systems. For such applications, the cabinets forming the power system in Fig. 5 are typically installed at distances below 100 m, and the network complexity is limited to few nodes. For example, in Section II, Fig. 4 shows four possible positions for the power transformers, plus one extra power transformer is needed in the case of connection to the high-voltage ac power line. The central supervising node may be installed in a control room, which can be placed at a distance of 100 m, a distance at which the CAN bus still provides a maximum data-rate up to 500 kb/s. The proposed diagnostic system can also be mounted on power transformers used on-board trains. In this case, the maximum distance covered by the CAN can be in the order of hundreds of meters, and the network complexity is in the order of tens of nodes. For such values of number of nodes and distance, the CAN approach is still well suited in an industrial environment. The USB connection, available for the diagnostic node in Fig. 7, is useful when the proposed diagnostic system is used as a standalone device to verify each power transformer before it is mounted in the power system.

The architecture of each MPN node in Fig. 7 entails three 3-axis capacitive Micro Electro Mechanical Systems accelerometers, with a bandwidth up to 1 kHz, a sensitivity of 0.5 mg, and a dynamic range configurable from ± 2 (the value set in our work) to ± 16 g. The LIS3DH sensors from STMicroelectronics have been adopted [37]. The power consumption in stand-by mode is limited to 7.2 μW:2 μA current with 3.6 V voltage supply.

Each sensor has also on-chip A/D converter and First In First Out buffers. Their digital outputs (16-b levels through a Serial Peripheral Interface connection) are time-multiplexed by the processing core, which is based on ARM CortexM3 CPU at 32 b plus 2 Mb of nonvolatile flash memory and roughly 1 Mb of RAM. The processing core runs at the maximum allowed frequency of 100 MHz. A 32-b 100-MHz unit has been selected versus less performing 8- or 16-b microcontrollers operating at few tens of megahertz since local signal processing has to be implemented.

For the diagnosis, the system works in the frequency domain. A 1024-point 16 b/sample fast Fourier transform (FFT) has been implemented softwarewise, for vibrational spectrum analysis plus arithmetic operator like maximum detection and threshold comparison. Since input acceleration data are sampled at $f_S = 2$ kHz, the length of the FFT has been selected as the power of two value (thus simplifying FFT design) that allows a frequency resolution of few hertz in the range of interest up to 1 kHz. Particularly, a 1024-point FFT (with 512 samples from dc to the Nyquist frequency, $f_S/2$) ensures a frequency resolution of 2 Hz. After FFT processing, a peak detection and thresholding unit allows the detection of the acquisition sequences potentially related to a mechanical degradation in the transformer. Each of these preselected sequences is compared to the reference vibration image acquired at the beginning of the transformer life cycle and stored in a nonvolatile memory. If the mean square of the difference with the reference sequence is above a given threshold, then a diagnostic alarm is raised. The thresholds are user programmable. The experimental measurements we have carried out (see Section V) prove that the difference between a good working transformer and one with degradation in the frequency domain is so high that the tuning of the thresholds is not an issue.

To be noted that the diagnostic system does not need strict real-time operations: for example, a software implementation of the FFT, peak-detection, thresholding, and comparison operations via software on the 32-b Cortex M3 core in Fig. 7 allows for a periodical check on a time scale of less than 10 min. This value is one order of magnitude better than what needed in practical applications, where a check each 100 min is enough.

The MPN node is equipped with on-board power supply regulators (providing the needed 3.3 V supply from external voltage levels up to 36 V) and with different types of possible network connection sustaining a data rate of hundreds of kilobits per second: wired connection through a CAN transceiver or wireless through an RF module. The RF part can work at 2.4 GHz using Bluetooth protocol or in the sub-gigahertz domain in Industrial Scientific Medical (ISM) unlicensed bands. To this aim, we reused a technology for antennas directly printed on the electronic PCB board we have first proposed in [38]. The covered connection distance is from few meters to several hundreds of meters. CAN networking is the preferred solution in industrial environments, although the availability of the RF links can be useful as redundant connection channels or for the deployment of such system in outdoor scenarios. The Stellaris Cortex M3 processing node

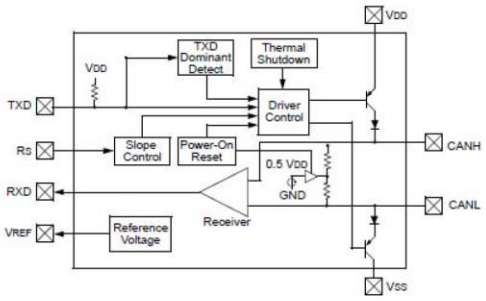

Fig. 8. CAN physical layer transceiver.

Fig. 9. Snapshot of the realized MPN node.

manages CAN communication at data link and networking layers but it needs an external transceiver to manage at physical layer differential CAN communications. The CAN physical layer is managed through the MCP2551 IC whose schematic is shown in Fig. 8.

An MPN unit can also be used stand-alone as a new instrument to check production quality before the power transformer is mounted on the power supply system and sold to the customer. In such a case, for each new power transformer, the vibration image is acquired and compared with a golden acceptance reference. If the check is passed, the transformer is mounted on the system, and the vibration image is used as a quality stamp and is provided with the rest of the technical documentation to the customer. To easy stand-alone use of the MNP node, it is also equipped with a USB interconnection (see Fig. 7). Fig. 9 shows a snapshot of the implemented system whose size is about 10 cm per side. The firmware has been developed using the IAR Embedded Workbench integrated development environment.

V. Experimental Measurements

A. Test System Calibration

To test the measuring system, first known sources of vibrations have been used. For example, Fig. 10 shows the performance of the Pico Vibe vibration motor [39], used to generate known source of vibrations in the frequency range [100 Hz, 300 Hz]. A similar approach has been used for preliminary tests of the measuring system in the [300 Hz, 1 kHz] frequency range. As already discussed in Section III, the frequency range of interest for diagnostic of degradations due to magnetostriction forces is from 100 Hz to 1 kHz. Particularly,

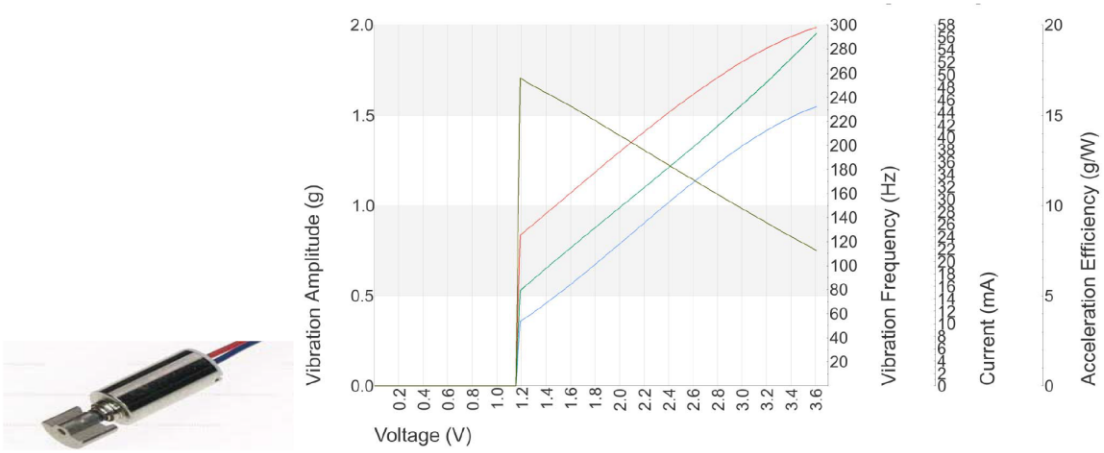

Fig. 10. Measured performance of the vibration motor used for the initial testing phase of the system as a function of the applied input voltage (red line: vibration frequency; blue line: vibration amplitude; green line: absorbed current; brown line: acceleration efficiency).

the red and blue lines in Fig. 10 show the amplitude and the frequency of the vibrations generated by the Pico Vibe motor as a function of its input voltage.

Fig. 10 also shows the absorbed current (green line) and the acceleration conversion efficiency (brown line) expressed as g/W. Driving the Pico Vibe vibration motor with a voltage from 1.2 to 3.6 V, we can generate vibrations up to 1.5 g in amplitude and up to 300 Hz in frequency. For example, with a 1.5 V input voltage, the Pico Vibe vibration motor generates a vibration with an amplitude of 0.5 g and a frequency of 150 Hz. The absorbed current is 20 mA and hence the power consumption is 30 mW. The acceleration conversion efficiency is above 15 g/W.

During this initial testing phase, vibrations generated by the Pico Vibe at different intensity and frequency levels have been measured through the diagnostic instrument, demonstrating a good alignment between generated and measured data.

B. Experimental Measurements on Real Power Transformers

Once the system has been tested, several experimental measurements have been carried out at CEG Elettronica premises on tens of real power transformers with different levels of degradation. Given the target application of railway signaling systems, the transformers used for the tests are of dry type. Tests have been done with both the power transformers with the secondary open or with the secondary connected to an active load (see Fig. 11) that allowed testing the device in tens of different electrical operating conditions. Comparing the results of these tests for the same power transformer allowed us to check if and how the measuring system performance depends on the operating condition of the device under test.

The accelerometers of each MNP unit have been placed in different positions of each power transformer under test to check if and how the diagnostic system performance depends on the sensors placement. Overall, thousands of tests have been carried out. For a sake of space, just some of them, we judge significantly to show how the diagnostic system

Fig. 11. Active load used during the measurement campaign to modify the operating conditions of each power transformer under test.

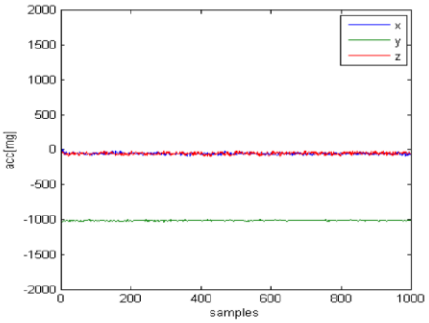

Fig. 12. Vibrations of a working power transformer. Sensors placed on top of the transformer tank. 90 A operating current (secondary).

behaves, are reported. Fig. 12 shows the response acquired when monitoring a power transformer without any fault or degradation. Vibrations are practically negligible; the y-axis is the vertical one on which the gravity acceleration (absolute

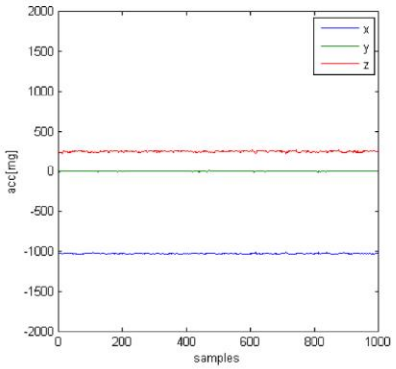

Fig. 13. Vibrations measured on a working power transformer with sensors directly connected to the transformer windings. 90 A operating current on the secondary.

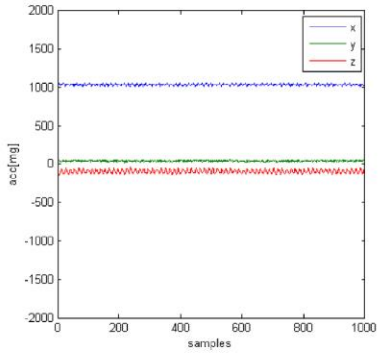

Fig. 14. Vibrations measured on a working power transformer with sensors directly connected to the transformer windings. 140 A operating current on the secondary.

value of 1 g) is measured. Repeating the same analysis with sensors placed on top of the power transformer tank, as shown in Fig. 12, or directly connected to the transformers windings, as shown in Fig. 13, similar results have been obtained. In Fig. 13, the three axes x, y, and z of the accelerometer have different static values than those in Fig. 12 since the position of the sensor is changed. The gravity acceleration is measured along the y-axis in the sensor placement of Fig. 12 and along the x-axis in that of Fig. 13. Data in Figs. 12 and 13 have been obtained with the transformer operating at a current of 90 A on the secondary.

Fig. 14 shows the measured accelerations on the same power transformer of Figs. 12 and 13 by changing both sensor position and operating conditions: the current is increased up to 140 A on the secondary.

From Fig. 14, it is clear that changing the operating conditions and the sensor positioning the amplitude of the vibrations around the static value imposed by the position of the sensor is limited to few milligrams for a good working transformer.

The results of Figs. 13 and 14 have been obtained with the three 3-axis accelerometers of each MPN unit directly connected each to one of the three transformer windings.

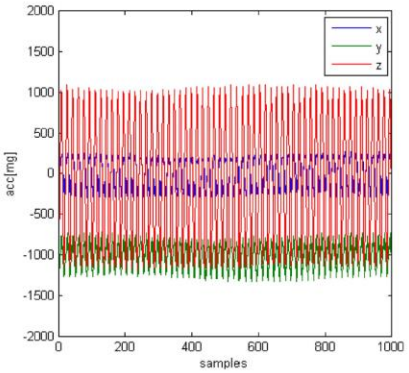

Fig. 15. Vibrations of a power transformer with degradation. Sensors placed directly on the transformer windings. 140 A operating current on the secondary.

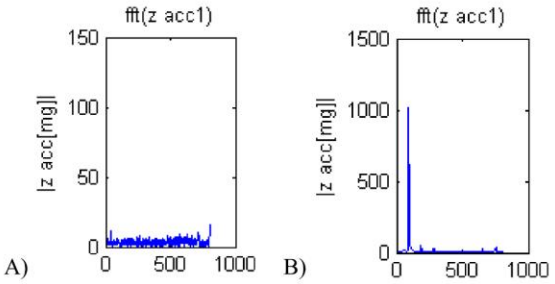

Fig. 16. Vibrations measured on a power transformer (z-axis, frequency domain) (A) without and (B) with degradation.

Similar values have been obtained from the three sensors; this work reports the value of the sensor measuring the highest vibration levels.

When repeating the same analysis on a power transformer with mechanical degradation, with sensors directly connected to the transformer windings, and with 140 A operating current on the secondary, the results of Fig. 15 are obtained. In Fig. 15, the degradation of the transformer can be clearly detected since the vibrations along the three axes are in absolute value up to 1 g (z-axis). Vibrations along the vertical y-axis have a lower intensity than those along the other axis due to the weight inertia of the transformer itself. Fig. 16 shows for the z-axis the same analysis of Figs. 14 and 15, but in the frequency domain: A) is the transformer without degradation whose measurements in time domain are in Fig. 14; B) is the transformer with mechanical degradation whose measurements in time domain are in Fig. 15.

Fig. 17 shows the two transformers under test (dry-type) referred to as A) and B) in Fig. 16.

Please note that for the transformer with degradation, case B) in Fig. 16, the FFT analysis reveals a peak at about 100 Hz. This value is twice the fundamental 50-Hz current frequency as expected from theory since magnetostriction forces in (1) are proportional to the square of the current. The peaks at multiple frequencies are much lower and the contribution near 1000 Hz or above is negligible.

Fig. 17. Transformers referred to as (A) (orange device on the left) and (B) (white device on the right) in Fig. 16.

Instead, the FFT figure is flat for the good-working transformer, case A) in Fig. 16.

The amplitude of vibrations is different from the case A), where the maximum level is within 10 mg, and the case B), where the maximum level is up to 1000 g. As consequence in Fig. 16, different ranges are used along the vertical axis.

For the transformer B) in Figs. 15 and 16 from a temperature, current and voltage measurement point of view, the behavior was perfectly aligned with the transformer labeled A). The measurements of audio emissions were also aligned between the two transformers although the vibration measurements in time and frequency domains (see Figs. 14–16) are quite different. This is due to the high noise level of the background industrial environment where the power transformers were positioned, more than 70 dB.

From a visual analysis, there are not particular differences to be noticed between A) and B) devices. Therefore, also a visual analysis is not suited for a predictive diagnosis unless the transformer comes to a complete degradation and is too late to prevent faults at system level.

Vibration measurement is the only way to detect the degradation, performing the measurements while the transformer is active, without any denial of service.

The only alternative to the approach proposed in this paper would be detecting the degradation through an invasive inspection, partially destructive, that forces a shutdown of the transformer and hence of the system.

In Fig. 18, the measurements on the power transformer B) with mechanical degradation have been repeated placing the sensors on top of the transformer tank. Both measurements in the time domain (Fig. 18) and in the frequency domain (Fig. 19) are reported.

By comparing the achieved results in Fig. 18 with those in Figs. 14 and 15 and by comparing the results in Fig. 19 with those in Fig. 16, the following are clear.

1) The degradation of the transformer is still clearly detectable since the amplitude of vibrations is up to 700 mg in Figs. 18 and 19, whereas for the transformer A) the worst case was that of Figs. 14 and 16(A) where the vibration amplitude is two orders of magnitude lower.
2) The sensitivity on the system by changing the position of the sensors is reduced by a 30% [along the z-axis, the amplitude of vibration is up to 700 mg in Figs. 18 and 19 while vibrations are up to 1 g in Figs. 15 and 16(B)].

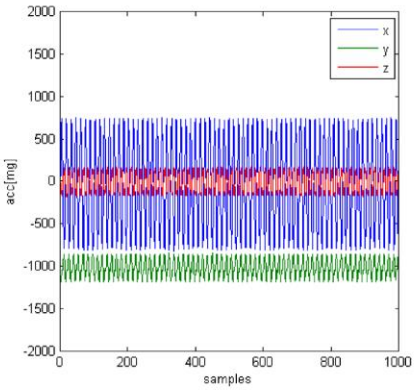

Fig. 18. Vibrations of a power transformer with degradation, sensor placed on top of the transformer tank, 140 A operating current on the secondary in the time domain.

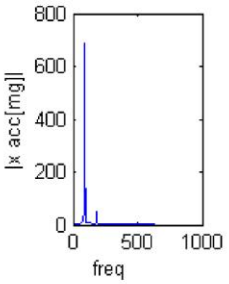

Fig. 19. Vibrations of a power transformer with degradation, sensor placed on top of the transformer tank, 140 A operating current on the secondary in the frequency domain.

In Fig. 19, we can notice a vibration peak of 700 mg at about 100 Hz, twice the 50 Hz current frequency as expected from (1), plus another small peak less than 50 mg at low frequency, whereas the contribution at frequencies above 200 Hz is less significant.

By repeating the measurements on the same transformer of Figs. 15 and 18, with the same sensor placement, but different operating conditions, the achieved results are the same. Therefore, there is a very low dependence of the system sensitivity on the operating conditions.

Another test has been applied to a whole power system with several transformers, where only one of them was affected by degradation. During the start sequence, all subblocks of the whole power supply system are sequentially activated. In such a case, the measuring system is a network of MPN units all communicating via CAN with the central monitoring unit, thus realizing a distributed diagnostic system.

Fig. 20 shows what is detected when the subblock is activated with the power transformers affected by degradation. The system visualizes the maximum vibrations among all the nodes so that even in case only one transformer starts degradation this condition is revealed. Then, through the CAN, the operator can remotely access each single power transformer and can analyze its vibration measure so that the faulty transformer can be isolated.

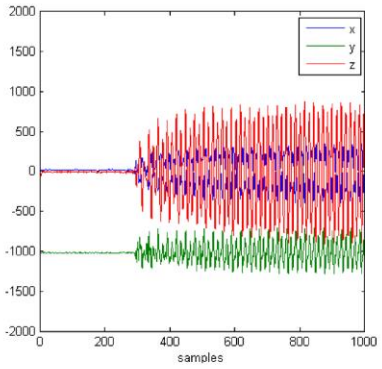

Fig. 20. Starting transient of a networked power system where one power transformer has degradation.

VI. Comparison to State of the Art

In summary, the proposed diagnostic system allows for monitoring complex power systems by revealing the degradation on power transformers not only by an electrical and thermal point of view, as in [24] and [40]–[49], but also by a mechanical point of view. For diagnosis of power transformers, just the measurement of some parameters is foreseen in most state-of-the-art works. For example, [43]–[44] and [49] measure the thermal coefficient of the insulation, the dielectric loss factor, partial discharges in the dielectric through a fiber Bragg grating (FBG) optical sensor (the sensor measures the shift in wavelength of FBG due to impulsive acoustic pressure generated during partial discharge event), and the stray reactance variations, respectively. Electrical measurements for power transformers are also proposed in [45]–[47], but mainly for the evaluation of no-load losses in [46] and [47], or for the evaluation of ratio error and phase angle error of a current transformer in [45], rather than for fault-detection or degradation analysis.

The diagnosis of the degradation is done in this work well in advance with respect to the time when a fault at system level occurs by revealing also, through vibration measurements, the mechanical degradation. As proved by our experimental tests, with an acoustic or visual analysis as in [23] and [50] of the transformer no degradations would be noticed. The proposed diagnostic system can be organized as a distributed network of local measurement and processing nodes, thus being scalable and easy adaptable to the power system size and physical placement. The diagnostic system can operate in real-time while the power system is working, thus avoiding any denial of service. Changing operating conditions of the transformer under test and the placement of sensors on the device under test do not affect the system capability to detect degradations. Indeed, between a good working transformer and one where degradations have started, there is a difference of at least two orders of magnitude in the measured vibrations in time and in frequency domain. Our proposed system is very simple to install and its cost is negligible if compared to the cost of the device under test since just three sensors are used for each device under test. Fault diagnosis of electrical machines using FFT analysis has been proposed in [51], but just limited to the analysis of rotating electrical machines in transient regime using the stator current.

Recent works have been proposed in [12]–[20] exploiting vibration measurements for mechanical fault diagnosis of power transformers. However, these systems use a much higher number of sensors, e.g., at least 10 in [13], 40 in [14], 8 in [15], 15 in [20], or 34 in [16] for each transformer instead of 3 in our solution. Recent works [12]–[17] and [19] adopt computation intensive algorithms, difficult to implement in low-cost embedded computing core as our work, and usually follow a centralized approach instead of the scalable networking approach proposed in this paper. Indeed, in [12] and [17], data from the sensors are acquired and then processed offline, for each transformer, on a dedicated workstation. For example, Wu *et al.* [19] propose a time-scale-frequency analysis for vibration measurements mixing Wavelet Packet and Hilbert Huang transforms, where the signal acquisition and processing is implemented for a single transformer through a dedicated acquisition board connected via USB to a general purpose computer implementing the signal processing chain. As consequence, such systems are limited to a stand-alone and offline use. In [18], [23], and [50], acoustic measurements are proposed as a diagnostic technique, but they are done in a controlled environment and not in the real operating one. For example, in [18], sonic waves due to vibrations in oil transformers are measured though in-oil hydrophone sensors in a laboratory setup, whereas [50] proposes a specific noise test chamber to measure the acoustic noise emitted by power transformers. As demonstrated by our test campaign with acoustic acquisition systems, the noise level of the real operating environment is high and hence an acoustic system will lead to a too high rate of missed detections.

This paper extends the WISP20015 contribution [7] where just a preliminary feasibility analysis was carried out. This work is extended both from the point of view of UPS design, since a new UPS scalable architecture has been proposed in Section II, and from the point of view of experimental assessment and comparison to the state of the art. Indeed, an exhaustive measurement campaign, missing in [7], is carried out in this work on real-power transformers with different degradation levels, operating conditions, and placements of the sensors.

VII. Conclusion

This work has addressed the problem of predictive diagnostic in three-phase high-power transformers. This paper is focused on their use in power systems with UPS capability for safety critical applications, such as railway interlocking signaling installations. A new scalable UPS architecture is presented too. A new instrumentation realized as a scalable networking of measuring nodes (vibration, thermal, and electrical characteristics), with integrated signal processing, is proposed for predictive diagnosis of mechanical, electrical, and thermal faults in power transformers. As innovative feature versus the state of the art, mechanical degradation is tracked through vibration measures, using multichannel accelerometers, with sensitivity down to 0.5 mg and local

processing in the transformed frequency domain up to 1 kHz. The performances of the diagnostic instrument, for which a compact hardware–software implementation is proposed, are assessed through experimental measurements on real dry-type high-power transformers used in railway applications. Changing operating conditions of the transformer under test and the placement of sensors on the device under test, do not affect the system capability to detect degradations. The proposed measuring system operates in real-time while the power system is working, thus avoiding any denial of service.

The measuring system allows predicting the mechanical degradation of power transformers when from audio or visual analysis the faults are still not noticeable.

Targeting a railway application, the CAN bus is selected as the main networking interface, providing a communication rate of hundreds of kilobits per second at several hundreds of meters [52]. The measuring and diagnostic nodes are equipped also with USB interface and with wireless communication links (2.4 GHz using Bluetooth protocol or in the subgigahertz domain in ISM unlicensed bands), thus increasing their flexibility. The new instrumentation can also be used for quality analysis of power transformer production: for each new power transformer, the vibration image is acquired and compared with a golden acceptance reference. If the check is passed, the transformer is sold and the vibration image is used as a quality stamp and provided to the customer with the technical documentation.

REFERENCES

[1] A. Consilvio, A. Di Febbraro, and N. Sacco, "A modular model to schedule predictive railway maintenance operations," in *Proc. Int. Conf. Models Technol. Intell. Transp. Syst. (MT-ITS)*, Budapest, Hungary, Jun. 2015, pp. 426–433.

[2] N. Costantino *et al.*, "Design and test of an HV-CMOS intelligent power switch with integrated protections and self-diagnostic for harsh automotive applications," *IEEE Trans. Ind. Electron.*, vol. 58, no. 7, pp. 2715–2727, Jul. 2011.

[3] H. M. Hashemian and W. C. Bean, "State-of-the-art predictive maintenance techniques," *IEEE Trans. Instrum. Meas.*, vol. 60, no. 10, pp. 3480–3492, Oct. 2011.

[4] R. Sunder, A. Kolbasseff, K. Kieninger, A. Röhm, and J. Walter, "Operational experiences with onboard diagnosis system for high speed trains," in *Proc. World Conf. Railway Res. (WCRR)*, 2001, pp. 1–9, paper 94.

[5] P. Umiliacchi, D. Lane, and F. Romano, "Predictive maintenance of railway subsystems using an ontology based modelling approach," in *Proc. World Conf. Railway Res. (WCRR)*, 2011, pp. 1–10.

[6] J. J. V. Antony and G. M. Nasira, "Towards predictive maintenance and management in rail sector: A clustering approach," in *Proc. IEEE Int. Conf. Recent Trends Inf. Technol. (ICRTIT)*, Jul. 2013, pp. 502–507.

[7] S. Saponara, L. Fanucci, F. Bernardo, and A. Falciani, "A network of vibration measuring nodes with integrated signal processing for predictive maintenance of high power transformers," in *Proc. IEEE WISP*, Siena, Italy, May 2015, pp. 1–4.

[8] D. Galar, A. Thaduri, M. Catelani, and L. Ciani, "Context awareness for maintenance decision making: A diagnosis and prognosis approach," *Measurement*, vol. 67, pp. 137–150, May 2015.

[9] K. Goebel, B. Saha, A. Saxena, J. R. Celaya, and J. P. Christophersen, "Prognostics in battery health management," *IEEE Instrum. Meas. Mag.*, vol. 11, no. 4, pp. 33–40, Aug. 2008.

[10] H. Gumilang *et al.*, "Condition assessment method for power transformer as a part of condition based maintenance program in PLN P3B Jawa Bali," in *Proc. IEEE Int. Conf. Condition Monitor. Diagnosis*, Sep. 2012, pp. 269–272.

[11] N. U. A. Wardani, A. P. Purnomoadi, H. I. Septiani, I. Arifianto, and B. Cahyono, "Condition assessment of 500/150 kV power transformer based on condition based maintenance," in *Proc. IEEE ICEEI*, Jul. 2011, pp. 1–4.

[12] H. Z. Ma, N. Jiang, C. N. Wang, and Z. H. Geng, "Improved power transformer winding deformation fault diagnosis method," *Appl. Mech. Mater.*, vol. 666, pp. 149–153, Oct. 2014.

[13] Y. Shao, Z. Rao, and Z. Jin, "Online state diagnosis of transformer windings based on time-frequency analysis," *WSEAS Trans. Circuits Syst.*, vol. 8, no. 2, pp. 227–236, 2009.

[14] C. Hu, P. Wang, B. D. Youn, W.-R. Lee, and J. T. Yoon, "Statistical health grade system against mechanical failures of power transformers," in *Proc. Conf. Prognostic Health Manage. Soc.*, 2012, pp. 1–13.

[15] P. H. Ibargüengoytia, R. Liñan, A. Pascacio, and E. Betancourt, "Probabilistic vibration models in the diagnosis of power transformers," in *Recent Advances in Vibrations Analysis*, N. Baddour, Ed. Rijeka, Croatia: InTech, 2011, ch. 6, pp. 103–122.

[16] J. T. Yoon, K. M. Park, B. D. Youn, and W.-R. Lee, "Diagnostics of mechanical faults in power transformers—Vibration sensor network design under vibration uncertainty," in *Proc. IEEE 2nd Eur. Conf. Prognostic Health Manage. Soc.*, 2014, pp. 1–7.

[17] M. Nafar, B. Bahmanifirouzi, and M. Jabbari, "Transformer monitoring by using vibration analysis," *Austral. J. Basic Appl. Sci.*, vol. 5, no. 11, pp. 984–990, 2011.

[18] M. Beltle and S. Tenbohlen, "Usability of vibration measurement for power transformer diagnosis and monitoring," in *Proc. IEEE Int. Conf. Condition Monitor. Diagnosis*, Sep. 2012, pp. 281–284.

[19] S. Wu *et al.*, "Extracting power transformer vibration features by a time-scale-frequency analysis method," *J. Electromagn. Anal. Appl.*, vol. 2, pp. 31–38, Jan. 2010.

[20] M. Jin, J. Pan, H. Huang, and J. Zhou, "Transmission of vibration of a power transformer from the internal structures to the tank," in *Proc. Acoust.*, Fremantle, WA, Australia, 2012, pp. 1–7.

[21] B. García, J. C. Burgos, and Á. M. Alonso, "Transformer tank vibration modeling as a method of detecting winding deformations—Part II: Experimental verification," *IEEE Trans. Power Del.*, vol. 21, no. 1, pp. 164–169, Jan. 2006.

[22] B. García, J. C. Burgos, and Á. M. Alonso, "Transformer tank vibration modeling as a method of detecting winding deformations—Part I: Theoretical foundation," *IEEE Trans. Power Del.*, vol. 21, no. 1, pp. 157–163, Jan. 2006.

[23] D. Y. Ming, "Research on fault diagnosis system for power transformer based on audio signal," M.S. thesis, Dept. Elect. Eng., Huazhong Univ. Sci. Technol., Wuhan, China, 2013.

[24] J.-W. Kim, B. Park, S. C. Jeong, S. W. Kim, and P. Park, "Fault diagnosis of a power transformer using an improved frequency-response analysis," *IEEE Trans. Power Del.*, vol. 20, no. 1, pp. 169–178, Jan. 2005.

[25] L. Hui, Z. Bin, C. Jiangbo, C. Chen, and W. Yang, "Simulation and test on vibration characteristics of power transformer windings," in *Proc. Int. Symp. Comput. Inform. (ISCI)*, 2015, pp. 1259–1267.

[26] S. Saponara, L. Fanucci, and A. Falciani, "Uninterruptible power supply systems for railway with predictive diagnostic against power transformer failure," in *Proc. IEEE 15th EEEIC*, Jun. 2015, pp. 2119–2123.

[27] G. M. Buiatti, J. A. Martín-Ramos, C. H. R. García, A. M. R. Amaral, and A. J. M. Cardoso, "An online and noninvasive technique for the condition monitoring of capacitors in boost converters," *IEEE Trans. Instrum. Meas.*, vol. 59, no. 8, pp. 2134–2143, Aug. 2010.

[28] J. Yu, "State-of-health monitoring and prediction of lithium-ion battery using probabilistic indication and state-space model," *IEEE Trans. Instrum. Meas.*, vol. 64, no. 11, pp. 2937–2949, Nov. 2015.

[29] D. Liu, W. Xie, H. Liao, and Y. Peng, "An integrated probabilistic approach to lithium-ion battery remaining useful life estimation," *IEEE Trans. Instrum. Meas.*, vol. 64, no. 3, pp. 660–670, Mar. 2015.

[30] M. V. Micea, L. Ungurean, G. N. Cârstoiu, and V. Groza, "Online state-of-health assessment for battery management systems," *IEEE Trans. Instrum. Meas.*, vol. 60, no. 6, pp. 1997–2006, Jun. 2011.

[31] L. C. Stevanatto, V. J. Brusamarello, and S. Tairov, "Parameter identification and analysis of uncertainties in measurements of lead–acid batteries," *IEEE Trans. Instrum. Meas.*, vol. 63, no. 4, pp. 761–768, Apr. 2014.

[32] E. R. Furlong, "UPS topologies for large critical power systems (>500 KVA)," in *Proc. 13th Annu. Power Quality Exhibit. Conf.*, 2002, pp. 1–9.

[33] N. Rasmussen, "The different types of UPS system," Vector, Mat 2012, pp. 62–64

[34] F. Baronti *et al.*, "State-of-charge estimation enhancing of lithium batteries through a temperature-dependent cell model," in *Proc. IEEE Int. Conf. Appl. Electron.*, Sep. 2011, pp. 1–5.

[35] A. Bonacchi and A. Fantechi, "Validation of interlocking systems by testing their models," in *Proc. 9th IEEE Int. Conf. Quality Inf. Commun. Technol.*, Sep. 2014, pp. 226–229.